



Tensor Network Calculation of the Logarithmic Correction Exponent in the XY Model

Seongpyo Hong¹ and Dong-Hee Kim^{1,2*}

¹Department of Physics and Photon Science, Gwangju Institute of Science and Technology, Gwangju 61005, Korea

²School of Physics, Korea Institute for Advanced Study, Seoul 02455, Korea

(Received May 14, 2022; accepted June 28, 2022; published online July 27, 2022)

We study the logarithmic correction to the scaling of the first Lee–Yang zero at the critical point in the classical XY model on square lattices by using tensor renormalization group methods. In comparing the higher-order tensor renormalization group (HOTRG) and the loop-optimized tensor network renormalization (LoopTNR), we find that the entanglement filtering in LoopTNR is crucial to gaining high accuracy for the characterization of the logarithmic correction, while HOTRG still proposes approximate upper and lower bounds for the zero location associated with two different bond-merging algorithms of the higher-order singular value decomposition and the oblique projectors. Using the LoopTNR data computed up to the system size of $L = 1024$ in the $L \times L$ lattices, we estimate the logarithmic correction exponent $r = -0.0643(9)$ from the extrapolation of the finite-size effective exponent, which is comparable to the renormalization group prediction of $r = -1/16$.

1. Introduction

Multiplicative logarithmic corrections appear in the critical behaviors of certain statistical physics models, introducing another set of scaling exponents characterizing criticality.^{1–3)} In the Berezinskii–Kosterlitz–Thouless (BKT) transition,^{4–7)} the renormalization group (RG) equations predicted that the correlation function $G(R)$ at the critical point exhibits the leading-order behavior^{7–9)} of $G(R) \sim R^{-\eta}(\ln R)^{-2r}$ or more generally $G(R) \sim R^{-\eta}(b + \ln R)^{-2r}$ with exponents $\eta = 1/4$ and $r = -1/16$ at a large distance R . The logarithmic correction factor essentially distinguishes the critical behaviors of the correlation function and susceptibility from those of the Ising model undergoing the second-order transition. On the other hand, it is numerically challenging to precisely identify such multiplicative logarithmic correction with a very small exponent. Much numerical effort has been devoted to measuring r in the two-dimensional (2D) XY model and related models undergoing the BKT transition.^{10–22)} While early estimates of r vary from positive to negative values (see Table 4 in Ref. 23), later large-scale Monte Carlo (MC) simulations showed improved agreement with the RG prediction.

In previous MC studies of the 2D XY model, Kenna and Irving¹⁰⁾ firstly measured $r = -0.02(1)$ from the finite-size-scaling (FSS) analysis of the lowest lying (first) Lee–Yang (LY) zero for system sizes up to $L = 256$ in the $L \times L$ square lattices. At the critical point, they found that the first LY zero θ_1 should behave with increasing system size L as

$$\theta_1 \sim L^\lambda (\ln L)^r, \quad (1)$$

which was derived from its relation to the leading-order scaling behavior of the susceptibility,

$$\chi \sim L^{-d} \theta_1^{-2} \sim L^{2-\eta} (\ln L)^{-2r}, \quad (2)$$

where $d = 2$ for two dimensions and thus $\lambda = -2 + \eta/2$. Using the Villain formulation, Janke¹⁵⁾ measured $r = -0.0270(10)$ from the FSS analysis of the susceptibility in the critical region for system sizes up to $L = 512$. Later, Hasenbusch²⁰⁾ examined an alternative scaling ansatz of the susceptibility,

$$\chi \sim L^{2-\eta} (C + \ln L)^{-2r}, \quad (3)$$

reporting $r = -0.056(7)$ from the FSS analysis with the MC dataset of $256 \leq L \leq 2048$ in the pure XY model. The high-temperature expansion done by Arisue²¹⁾ reported the similar value of $r = -0.054(10)$ from the calculation of the moments of the correlation function. Most recently, Komura and Okabe²²⁾ performed large-scale MC calculations for sizes up to $L = 65536$, reporting the best fit with $r = -0.064(4)$ at the fixed value of $C = \ln 16$ in the FSS analysis of the susceptibility. The parameter C effectively includes subleading-order corrections that may decay rather slowly with increasing L .²⁰⁾ Setting $C = 0$ provided smaller values of $r = -0.0406(3)$ in Ref. 20 and $r \approx -0.55$ in Ref. 22 with similar system sizes.

In this paper, we revisit the FSS analysis of the first LY zero in the 2D XY model by employing methods based on the tensor renormalization group (TRG). Since the first MC measurement of the LY zero,¹⁰⁾ there have been no other attempts to measure the logarithmic correction exponent using the LY zero in the XY model. Most of other previous estimates of r were based on the susceptibility that might have been more straightforwardly measurable in cluster MC simulations. The purpose of the present work is to examine applicability of the TRG-based methods to the numerical identification of the first LY zero and then to provide an updated estimate of the logarithmic correction exponent.

The TRG methods provide a deterministic way of evaluating the partition function of a classical spin model in the tensor network representation.²⁴⁾ The higher-order tensor renormalization group (HOTRG) method²⁵⁾ was previously applied to the Fisher zero problem where the partition function is evaluated at a complex temperature.^{26,27)} In the Ising and Potts models, the HOTRG method was also used to obtain the density of the LY zeros from the discontinuity of magnetization.²⁸⁾ While tensor network methods have been actively applied to study phase transitions in classical and quantum systems,²⁹⁾ including the BKT transitions,^{30–37)} the computation of the first LY zero in the XY model has not been studied with TRG yet. It still remains unclear whether or not a TRG-based method such as HOTRG

allows enough accuracy to characterize such delicate logarithmic correction with a small exponent predicted at the BKT transition.

We compare HOTRG with the loop-optimized tensor network renormalization (LoopTNR)³⁸⁾ in identifying the location of the first LY zero at the critical point. It turns out that HOTRG fails to give a converged estimate at a large system, although it still proposes approximate bounds for the zero location that are set by the estimates associated with two different bond-merging algorithms based on the higher-order singular value decomposition²⁵⁾ and the oblique projector method.³⁹⁾ In contrast, the LoopTNR calculations show much better convergence with increasing the bond dimension cutoff, indicating the importance of removing the short-range entanglement.⁴⁰⁾ We obtain the first LY zeros for system sizes up to $L = 1024$ in the XY model. In the analysis of the alternative scaling ansatz with an undetermined constant as being introduced in the susceptibility,²⁰⁾ we present that our finite-size estimate of the logarithmic correction exponent approaches closer to the RG prediction, providing the updated estimate of $r = -0.0643(9)$ from extrapolation.

This paper is organized as follows. In Sect. 2, we describe the numerical procedures including a brief review of HOTRG and the two bond-merging algorithms and the performance of our initial state preparation for the loop optimization in the LoopTNR calculations. In Sect. 3, we present the comparison between the two bond-merging algorithms of HOTRG and the estimate with LoopTNR in computing the first LY zero and the analysis of the LoopTNR data of the LY zero to measure the logarithmic correction exponent in the XY model. Summary and conclusions are given in Sect. 4.

2. Numerical Procedures

2.1 XY model and Lee–Yang zeros

The classical XY model is described by the Hamiltonian,

$$H = -J \sum_{\langle i,j \rangle} \cos(\phi_i - \phi_j) - h \sum_i \cos \phi_i, \quad (4)$$

where ϕ_i is a spin angle at site i , and h denotes a magnetic field. The coupling strength J and the Boltzmann factor k_B are set to be unity, and thus the temperature unit J/k_B and the magnetic field unit J are omitted for brevity throughout this paper. We consider the periodic boundary conditions.

The zeros of a partition function provide an alternative tool to study phase transitions and critical phenomena (see, for instance, Refs. 41 and 42 and references therein). The LY zeros^{43,44)} are defined in the plane of complex fugacity while the Fisher zeros⁴⁵⁾ are defined in the plane of complex temperature. Characterizing the BKT transition using partition function zeros has been interest of many previous works.^{10–12,26,27,46–50)} In the models that satisfy the Lee–Yang theorem,⁴⁴⁾ including the XY model,⁵¹⁾ the LY zeros are exactly on the imaginary axis of the magnetic field. The first LY zero is the one with the smallest magnitude, exhibiting a characteristic scaling behavior with increasing system size at the critical point.

Finding the location of the LY zero requires the evaluation of the partition function $Z = \sum_{\{\phi_i\}} \exp(-\beta H)$ at an imaginary magnetic field $h = i\theta$. In the XY model, we fix the inverse temperature β at the critical point $\beta_c = 1.1199$ that is agreed between the previous large-scale Monte Carlo,^{20,22)}

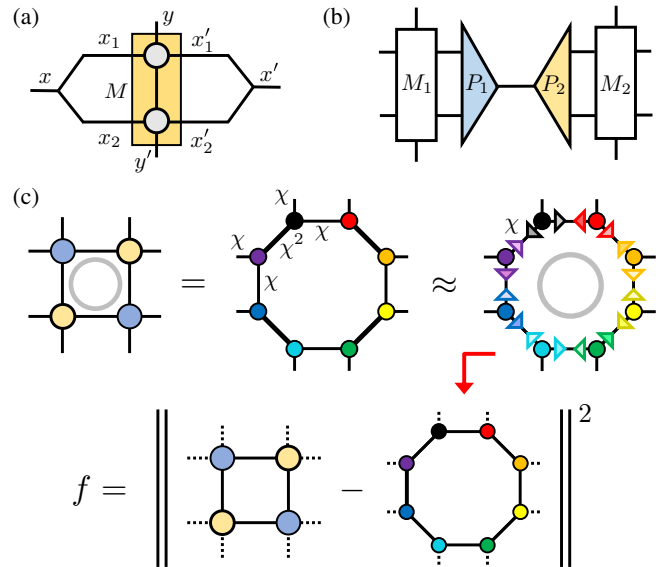


Fig. 1. (Color online) Schematic diagram of (a) the combine tensor M in HOTRG, (b) the oblique projectors, and (c) the initial tensor preparation for the loop optimization in LoopTNR. In (c), thicker bonds have dimension as large as χ^2 that is to be truncated by the projectors of the entanglement filtering.

high-temperature expansion,²¹⁾ and tensor network renormalization³⁷⁾ studies. To identify the first LY zero θ_1 , we first graphically locate an approximate location of θ_1 and then numerically minimize $|Z(\beta_c, \theta)|$ to refine the estimate of θ_1 .

In the TRG formulation,²⁴⁾ the partition function of a classical spin model with local interactions is written in the square lattices as

$$Z(\beta_c, \theta) = \text{Tr} \prod_i T_{x_i x'_i y_i y'_i}, \quad (5)$$

where T is a local tensor, and its four legs are associated with the bonds in the x and y directions. In the XY model, the local tensor is given as^{30,52)}

$$T_{xx'yy'} = \sqrt{I_x(\beta_c)I_{x'}(\beta_c)I_y(\beta_c)I_{y'}(\beta_c)} I_{x+y-x'-y'}(i\beta_c\theta), \quad (6)$$

where I_n is the modified Bessel function of the first kind. While the exact enumeration of the tensor product in Eq. (5) is numerically impossible unless the system is very small, TRG provides a controlled way to compute Z by coarse-graining the tensor network with bond dimension truncation. Below we briefly describe the procedures of the two TRG-based methods that we employ to evaluate the partition function.

2.2 HOTRG and bond-merging methods

An essential part of the HOTRG procedures is the step of merging a pair of parallel bonds into a one bond in the contraction of two neighboring tensors. In the square lattices of $2^N \times 2^N$ sites, with translation invariance being imposed, the final coarse-grained tensor is obtained by performing $2N$ contractions alternatively along the x and y directions. For instance, as shown in Fig. 1(a), one can write down the contraction of two neighboring tensors along the y direction as

$$M_{xx'yy'} = \sum_i T_{x_1 x'_1 y_i} T_{x_2 x'_2 i y'}, \quad (7)$$

where the bond dimension of $x \equiv x_1 \otimes x_2$ and $x' \equiv x'_1 \otimes x'_2$ increases to χ^2 if each leg of T has dimension χ . The crucial part of HOTRG is to keep the dimension of x and x' below a numerically manageable cutoff χ . The truncation error is due to the finite cutoff limited by available computing resources.

The original HOTRG paper²⁵⁾ proposed the higher-order singular value decomposition (HOSVD) for the truncation as

$$T'_{xx'yy'} = \sum_{ij} U_{ix} M_{ijyy'} U_{jx'}^*, \quad (8)$$

where the matrix U is determined by solving an eigenproblem of MM^\dagger . To preserve the symmetry of the local tensor at an imaginary magnetic field, we perform the orthogonal transformation by diagonalizing the real part of MM^\dagger in the same way that was used in Refs. 26 and 27 for the Fisher zero problem.

The other bond-merging algorithm³⁹⁾ considers a pair of the oblique projectors P_1 and P_2 inserted between the neighboring combined tensors M_1 and M_2 , as sketched in Fig. 1(b), minimizing $\|M_1 M_2 - M_1 P_1 P_2 M_2\|$ at a given cutoff χ of the bond dimension between them. While details of the algorithm can be found in the literature,^{39,53,54)} let us briefly review the numerical procedures. The projectors are given as

$$P_1 = R_2 \tilde{V}_t \tilde{\Sigma}_t^{-1/2}, \quad (9)$$

$$P_2 = \tilde{\Sigma}_t^{-1/2} \tilde{U}_t^\dagger R_1, \quad (10)$$

where R_1 and R_2 are from the QR and RQ factorization of M_1 and M_2 , respectively, and the other tensors are from the truncated singular value decomposition (SVD) of $R_1 R_2 \approx \tilde{U}_t \tilde{\Sigma}_t \tilde{V}_t^\dagger$ that keeps the largest χ singular values. The R tensors can be computed using matrix diagonalization as

$$R_1 = \Lambda_1^{1/2} U_1, \quad (11)$$

$$R_2 = U_2^\dagger \Lambda_2^{1/2}, \quad (12)$$

where $M_1^\dagger M_1 = U_1^\dagger \Lambda_1 U_1$ and $M_2 M_2^\dagger = U_2^\dagger \Lambda_2 U_2$. Finally, the contraction along the y direction is done as

$$T'_{xx'yy'} = \sum_{ij} [P_2]_{xi} M_{ijyy'} [P_1]_{jx'}. \quad (13)$$

While the symmetry of the local tensor in Eq. (6) is not explicitly preserved with the oblique projectors at a complex field, the first LY zero computed using the projectors shows accuracy comparable to the symmetry-preserved HOSVD. These two bond-merging algorithms play complementary roles in the search for the LY zero location. It turns out that they provides approximate upper and lower bounds for the true zero location, which we will demonstrate later in Sect. 3.

2.3 Loop optimization of tensor network renormalization

A known issue of TRG is that it does not make an isolated RG flow because of the survival of the short-range entanglement.⁴⁰⁾ HOTRG is much more accurate than the original TRG at a non-critical region, but it also suffers from the same issue of the original TRG at a critical point, which may cause inaccuracy in finding the LY zero especially at a large system. Several methods^{38,40,55–58)} have been proposed to remove the short-range entanglement and demonstrated that a correct fixed point tensor is recovered with much higher accuracy at a critical point. So far, the effect of the

entanglement filtering remains untested in the plane of a complex field or temperature for a partition function zero problem. In Sect. 3, we will show that removing the short-range entanglement is crucial particularly to the identification of the multiplication logarithmic correction in the XY model.

We adopt the LoopTNR method³⁸⁾ that extends the TRG scheme by adding the entanglement filtering step to remove the corner double line tensors and replacing the truncated SVD of the original TRG with the loop optimization. We have implemented our code by faithfully following the original paper³⁸⁾ yet with extra care of preparing an initial tensor for the loop optimization. It was already pointed out in the original paper that choosing a good initial tensor could considerably speed up the convergence of iterations in the loop optimization.

The simplest way of preparing an initial octagonal tensor ring for the loop optimization is to perform the truncated SVD as done in the original TRG scheme. Instead, as sketched in Fig. 1(c), we use the entanglement filtering algorithm to generate projectors to truncate the bond dimension. We first apply SVD to the local tensors with all singular values being kept and then perform the entanglement filtering on the eight-tensor ring. In the final step, the projectors are constructed by choosing the largest χ singular values. During the loop optimization, the entanglement filtering is performed every ten sweeps for better stability. The maximum number of sweep is limited to 200. Figure 2 presents comparison between two choices of the initial tensors, showing that the entanglement filtering projectors gains order-of-magnitude improvement over the simple truncated SVD in the minimization of the cost function.

3. Results and Discussion

3.1 Comparison between HOTRG and LoopTNR

We compare the cutoff dimension dependence of the LY zero estimates computed using HOTRG and LoopTNR. Our findings in the following are based on common observations in the Ising and XY models. First, in the HOTRG calculations, two bond-merging algorithms approach each other from the opposite sides as the cutoff χ increases. While it fails to converge, the comparison between the estimates associated with the two bond-merging algorithms proposes the upper and lower bounds for the zero location. Second, LoopTNR converges much faster than HOTRG and thus provides a more reliable estimate of the zero location. The comparison between HOTRG and LoopTNR shows the importance of the entanglement filtering to the precise identification of the LY zeros in the XY model.

Figure 3 displays the first LY zeros computed in the 2D Ising model. The LoopTNR calculations verify the exact scaling behavior $\theta_1(L) \propto L^\lambda$ with the critical exponent $\lambda = -15/8$ at a relatively low cutoff $\chi = 14$. On the other hand, the HOTRG calculations converge rather slowly with increasing χ , which gets worse as it goes to larger systems. Interestingly in the HOTRG calculations, the direction of the LY zeros moving toward the exact scaling line with increasing χ depends on which bond-merging algorithm is used. While the one with HOSVD approaches the exact scaling line of the first LY zero from above, the other with the oblique projectors lies below the exact line, proposing an area where the exact LY zero should be located. Although our

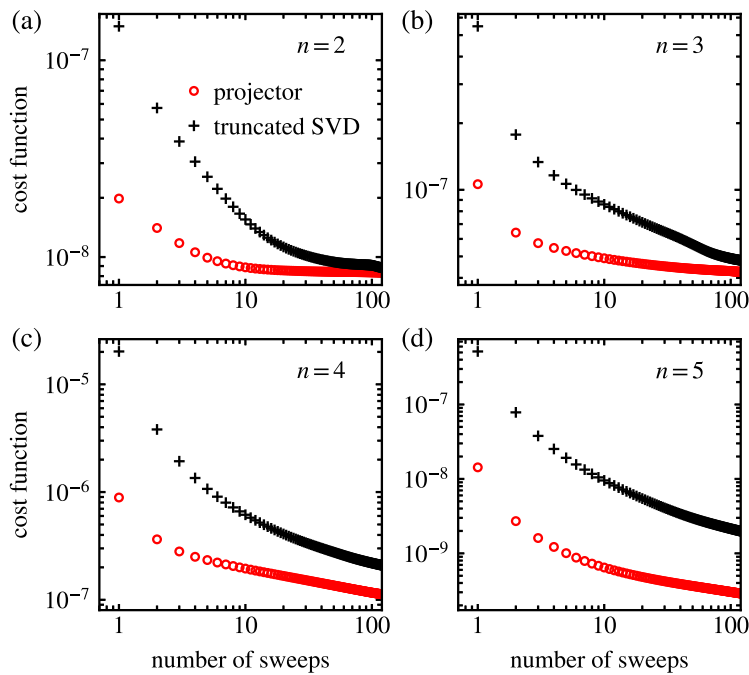


Fig. 2. (Color online) Convergence of the loop optimization. The cost function f is plotted as a function of the number of sweeps in the loop optimization tested at the n -th coarse-graining step in the 2D XY model. The marker with “projector” represents our initial tensor preparation method where the truncation occurs with the entanglement filtering. The other marker represents the initial tensor prepared by the truncated SVD of the TRG scheme. The calculations are done at $\beta = \beta_c$ and $h = i$ with the bond dimension cutoff $\chi = 40$.

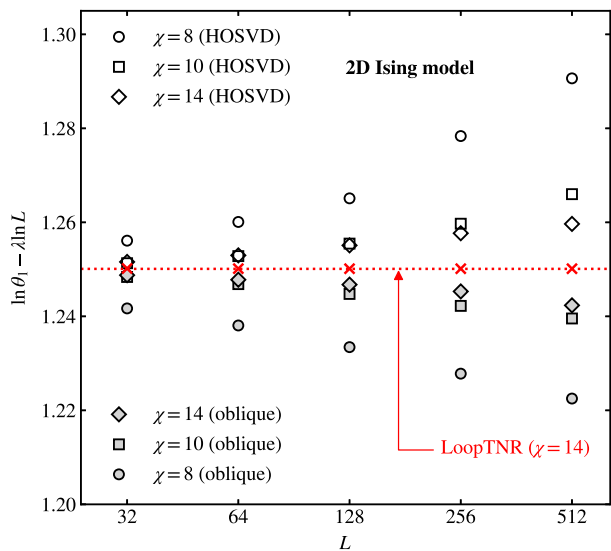


Fig. 3. (Color online) Comparison between HOTRG and LoopTNR in finding the first LY zero of the 2D Ising model at the critical point. Different cutoff values of the bond dimension ($\chi = 8, 10, 14$) are examined with the HOSVD and oblique projector methods in the bond-merging step of HOTRG. The exponent λ is fixed at $-15/8$. The dotted line indicates the exact scaling behavior.

observation is purely empirical, testing the different bond-merging algorithms may help judging the absolute convergence of the LY zero estimate. In the Ising model, one can simply increase χ to see that the two HOTRG estimates indeed meet each other on the exact scaling line for the system sizes shown in Fig. 3.

Figure 4 shows the same tendency with the bond-merging algorithms of the HOTRG estimates in the XY model. The zero estimate moves with increasing χ from the opposite

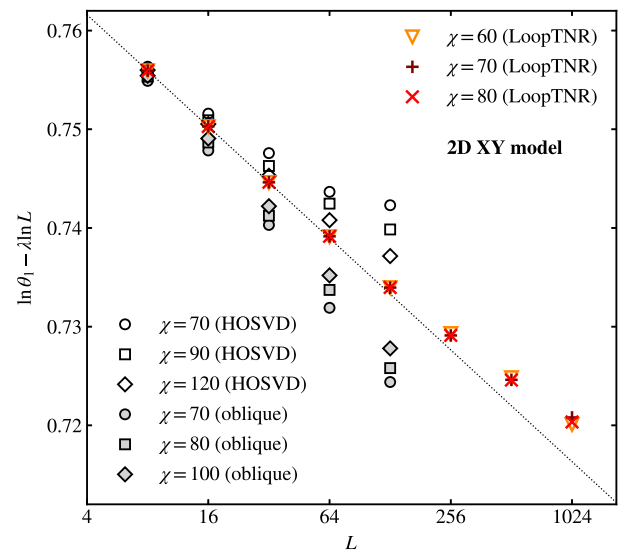


Fig. 4. (Color online) First LY zero of the 2D XY model at the critical point $\beta_c = 1.1199$. The LoopTNR results are compared with the HOTRG estimates based on the HOSVD and oblique projector methods. The exponent λ is fixed at $-15/8$. The dotted line of $L^{-0.0082}$ is given for comparison with a pure power law.

directions associated with the two bond-merging algorithms. The situation in the XY model is in fact much worse than in the Ising model. We fail to make these two HOTRG estimates meet together for $L \geq 16$ even at the largest cutoff that we have examined. Thus, it is not practically possible to study the multiplicative logarithmic correction to the scaling of the LY zero by using the HOTRG calculations.

In contrast, the estimates of the LY zeros from the LoopTNR calculations with the cutoffs of $\chi = 60, 70, 80$ graphically overlap onto each other. All are well within the

Table I. Numeric data of the first LY zero computed using the LoopTNR method with the bond dimension cutoff $\chi = 60, 70, 80$ in the 2D XY model.

L	$\chi = 60$	$\chi = 70$	$\chi = 80$
8	0.043152022481	0.043152341820	0.043152516125
16	0.011697992784	0.011698219091	0.011698141443
32	0.003171206193	0.003171237666	0.003171264869
64	0.000859814590	0.000859847214	0.000859849347
128	0.000233203560	0.000233203767	0.000233206505
256	0.000063265430	0.000063270187	0.000063270583
512	0.000017175547	0.000017171787	0.000017171295
1024	0.000004660332	0.000004663680	0.000004661544

bounds proposed by the HOTRG estimates. While the convergence with different χ 's is not perfect for the largest L as seen in the numeric data of the LY zeros listed in Table I, the larger bond dimension makes the less truncation error in building a coarse-grained tensor and should provide the more accurate data. Our measurements of the exponent r of the multiplicative logarithmic correction to the scaling presented below are mainly based on the data of the largest cutoff $\chi = 80$ that we have managed to reach in our LoopTNR calculations.

3.2 Logarithmic correction exponent

We measure the logarithmic correction exponent r by examining two possible forms of the FSS ansatz. First we examine the ansatz of the asymptotic scaling behavior,

$$\theta_1(L) \sim L^\lambda (\ln L)^r, \quad (14)$$

which is the same one considered in the previous MC study of the LY zero in the XY model.¹⁰ In finite-size systems, there must be an influence from non-universal subleading-order terms that decay with increasing L . This finite-size effect is expected to be particularly problematic when trying to identify the logarithmic correction exponent because its base is the logarithm of the system size. An ideal FSS analysis to determine the exponent r would need a dataset of very large system sizes, such as a series of $\log_2 L = 2^n$, to perform a conventional log-log fit. However, the sizes allowed in our calculations are $l \equiv \log_2 L = 3, 4, 5, \dots, 10$, implying that a significant finite-size effect could appear in the evaluation of the exponent.

The LoopTNR calculation is deterministic at a given bond dimension cutoff χ and free from a stochastic uncertainty. If the LoopTNR data of the first LY zero is precise enough, a good way to get an exponent can be extrapolating the finite-size exponents that are computed by equating r in Eq. (14) with two different system sizes. Which is extrapolated toward the wanted exponent r in the thermodynamic limit. This method is sensitive to the accuracy of the raw data and thus typically used for numerically exact data at small systems. We write the finite-size exponent r_{eff} by choosing two consecutive system sizes of l and $l + 1$ as

$$r_{\text{eff}}(l) = \left(\log_2 \frac{\theta_1(l+1)}{\theta_1(l)} - \lambda \right) / \log_2 \left(1 + \frac{1}{l} \right), \quad (15)$$

where λ is fixed at $-15/8$. Supposed no numerical error existing in $\theta_1(l)$, the finite-size behavior of $r_{\text{eff}}(l)$ is solely due to the subleading-order contributions that decrease with increasing l , implying that r_{eff} monotonically approaches the exact value of the exponent r as l increases.

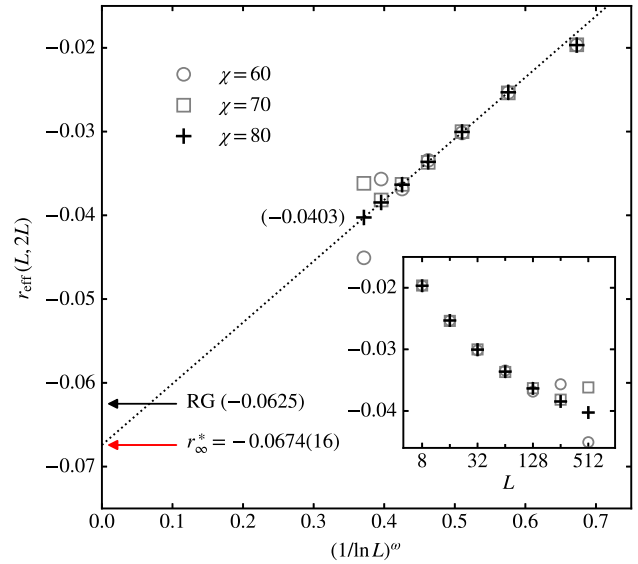


Fig. 5. (Color online) Logarithmic correction exponent estimate based on the scaling ansatz of $\theta_1 \propto L^\lambda (\ln L)^r$. The exponent λ is fixed at $-15/8$. The finite-size exponent r_{eff} is computed for every consecutive sizes of $(L, 2L)$ using the LoopTNR data of $\chi = 60, 70, 80$. The extrapolation along the line of $r_{\text{eff}}(L) = r_\infty^* + a(\ln L)^{-\omega}$ is shown at the parameter $\omega = 0.541$ obtained from a fit to the data points of $\chi = 80$ with $L = 8$ being excluded.

Figure 5 presents $r_{\text{eff}}(l)$ obtained from the two-point estimate of Eq. (15). It turns out that the data with the largest cutoff available ($\chi = 80$) shows a smooth monotonic curve expected in this method while the less accurate ones with the lower cutoffs indicate deviations from the one with the largest cutoff at $L = 512$ and 1024 . We perform the extrapolation with the data of $\chi = 80$ along the model line of

$$r_{\text{eff}}(l) = r_\infty^* + a_o l^{-\omega}, \quad (16)$$

finding $r_\infty^* = -0.0674(16)$. Although this number is close to the RG prediction $r_{\text{RG}} = -0.0625$, we must point out the risks of such extrapolation. This extrapolation model assumes decay in the form of $l^{-\omega}$, which lacks a theoretical ground. In addition, the available data points are quite far from the intercept at $1/l = 0$ on the extrapolation line, implying that the intercept r may significantly vary with a choice of the model. While this issue is fundamental, we argue that it is less severe if we take the alternative ansatz with an undetermined constant.

In the FSS analysis of the BKT transition, the logarithmic correction is often described by $(C + \ln L)$ with an undetermined constant C instead of $\ln L$.^{20,59} Similarly, we may write the system-size scaling ansatz of the first LY zero as

$$\theta_1(L) \sim L^\lambda (C + \ln L)^r, \quad (17)$$

where the constant C may help us to include some of subleading-order contributions within the ansatz. To determine the two unknowns of r_{eff} and C , we need to consider three system sizes $(l, l + 1, l + 2)$. The equation for $c \equiv C/\ln 2$ is then written as

$$\frac{\log_2 \frac{\theta_1(l+1)}{\theta_1(l)} - \lambda}{\log_2 \frac{\theta_1(l+2)}{\theta_1(l+1)} - \lambda} = \frac{\log_2 [1 + (c+l)^{-1}]}{\log_2 [1 + (c+l+1)^{-1}]}, \quad (18)$$

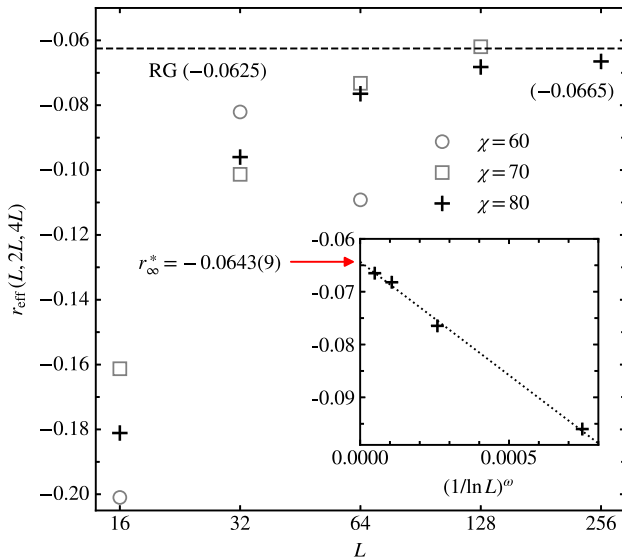


Fig. 6. (Color online) Logarithmic correction exponent estimate based on the scaling ansatz of $\theta_1 \propto L^\lambda(C + \ln L)^\nu$. The exponent λ is fixed at $-15/8$. The finite-size logarithmic correction exponent r_{eff} is computed with three system sizes of $(L, 2L, 4L)$ in the LoopTNR data of $\chi = 80$. The extrapolation along the line of $r_{\text{eff}}(L, 2L, 4L) = r_\infty^* + a(\ln L)^{-\omega}$ is shown at the fitting parameter of $\omega = 5.79$ obtained with the data point of $L = 8$ being excluded.

which is to be solved numerically. The right-hand side is a bounded and monotonic function of c , indicating that there exists a single solution or no solution. Once c is determined, the finite-size exponent r_{eff} can be computed as

$$r_{\text{eff}}(l) = \left(\log_2 \frac{\theta_1(l+1)}{\theta_1(l)} - \lambda \right) / \log_2 \left(1 + \frac{1}{c+l} \right). \quad (19)$$

Figure 6 shows r_{eff} obtained from the three-point analysis of Eqs. (18) and (19). As one may have expected already in the two-point analysis, the datasets of $\chi = 60, 70$ having larger truncation errors do not give a solution of c at large L 's. In contrast, the dataset of $\chi = 80$ provides a solution for c at all l 's examined. The three-point estimate of r_{eff} seems to saturate faster as l increases than the two-point estimate without C , which may be seen from the value of $\omega = 5.7$ in the extrapolation along the line of Eq. (16), while it was $\omega = 0.541$ in the case of the two-point analysis. The intercept $r_\infty^* = -0.0643(9)$ is close to the data of $r_{\text{eff}} = -0.0665$ obtained at the largest l and is also well compared to the RG prediction.

Finally, it is also worth to note that our dataset proposes a possible range of r without extrapolation being attempted. As displayed in Figs. 5 and 6, the two-point estimate of r_{eff} monotonically decreases with increasing l while the three-point estimate increases with l . The two curves have to meet at a true value of r in the limit of infinite l . Therefore, these monotonic yet contrasting behaviors of $r_{\text{eff}}(l)$ observed in the two different analysis indicate that the exact r must be in the range of $-0.0665 < r < -0.0403$, where the numbers are given by r_{eff} at the largest l available in Figs. 5 and 6. This range is probably the most conservative measure of r that we can provide, although the power-law extrapolation suggests that the true r is likely to be much closer to the lower bound of the range.

4. Summary and Conclusions

We have investigated the applicability of the TRG-based methods of HOTRG and LoopTNR to the calculation of the first LY zero, with a particular focus on the multiplicative logarithmic correction to the scaling at the critical point in the 2D XY model. It turns out that while LoopTNR exhibits graphical convergence in the LY zero location, HOTRG fails to provide a reliable estimate within our accessible bond dimension cutoffs, assuring the importance of the entanglement filtering in LoopTNR. Despite the failure of HOTRG, we have found that the opposite convergence directions associated with the two different bond-merging algorithms of HOSVD and the oblique projectors can propose the bounds for the zero location between which the LoopTNR estimate indeed resides.

By using the LoopTNR dataset of the first LY zeros, we have measured the logarithmic correction exponent r in the XY model. We have considered the finite-size effective exponent r_{eff} that is computed from a adjacent set of of the LY zero data. In the two- and three-point analysis of r_{eff} based on the two types of a scaling ansatz, we have identified the range of $-0.0665 < r < -0.0403$ at the largest system size examined for the measure of the exponent. The extrapolation with the three-point estimates provides $r_\infty^* = -0.0643(9)$ that is well compared to the RG-predicted value of $r = -0.0625$.

Our estimates of r are based on the LoopTNR dataset of $\chi = 80$ that is the largest cutoff accessible within our computing resources. The irregularity observed at the lower values of the cutoff implies that $\chi = 80$ may be the minimum bond dimension cutoff for LoopTNR to achieve enough accuracy required to the proper characterization of the multiplicative logarithmic correction. While it is computationally challenging to increase χ further larger in the present study, our three-point analysis method of computing r_{eff} based on the ansatz of Eq. (17) can be a benchmark for future tensor network calculations at larger values of χ to pursue a more precise measurement of the logarithmic correction exponent in the XY model and other systems undergoing the BKT transition.

Acknowledgments The authors are grateful to Katharine Hyatt for guidance in using the GPU-accelerated ITensor⁶⁰ library. This work was supported from the Basic Science Research Program through the National Research Foundation of Korea funded by the Ministry of Science and ICT (NRF-2019R1F1A106321). Computing resources are provided by the KISTI supercomputing center (KSC-2021-CRE-0165).

*dongheekim@gist.ac.kr

- 1) R. Kenna, D. A. Johnston, and W. Janke, *Phys. Rev. Lett.* **96**, 115701 (2006).
- 2) R. Kenna, D. A. Johnston, and W. Janke, *Phys. Rev. Lett.* **97**, 155702 (2006).
- 3) R. Kenna, in *Order, Disorder and Criticality*, ed. Y. Holovatch (World Scientific, Singapore, 2012) Vol. 3, p. 1.
- 4) V. L. Berezinskii, *Sov. Phys. JETP* **32**, 493 (1971).
- 5) J. M. Kosterlitz and D. J. Thouless, *J. Phys. C* **5**, L124 (1972).
- 6) J. M. Kosterlitz and D. J. Thouless, *J. Phys. C* **6**, 1181 (1973).
- 7) J. M. Kosterlitz, *J. Phys. C* **7**, 1046 (1974).
- 8) D. J. Amit, Y. Y. Goldschmidt, and S. Grinstein, *J. Phys. A* **13**, 585 (1980).
- 9) L. P. Kadanoff and A. B. Zisook, *Nucl. Phys. B* **180**, 61 (1981).

- 10) R. Kenna and A. Irving, *Phys. Lett. B* **351**, 273 (1995).
- 11) A. C. Irving and R. Kenna, *Phys. Rev. B* **53**, 11568 (1996).
- 12) R. Kenna and A. C. Irving, *Nucl. Phys. B* **485**, 583 (1997).
- 13) A. Patrascioiu and E. Seiler, *Phys. Rev. B* **54**, 7177 (1996).
- 14) M. Campostrini, A. Pelissetto, P. Rossi, and E. Vicari, *Phys. Rev. B* **54**, 7301 (1996).
- 15) W. Janke, *Phys. Rev. B* **55**, 3580 (1997).
- 16) A. Jaster and H. Hahn, *Physica A* **252**, 199 (1998).
- 17) Y. Tomita and Y. Okabe, *Phys. Rev. B* **65**, 184405 (2002).
- 18) S. Chandrasekharan and C. G. Strouthos, *Phys. Rev. D* **68**, 091502 (2003).
- 19) C. G. Strouthos, *Nucl. Phys. B (Proc. Suppl.)* **129–130**, 608 (2004).
- 20) M. Hasenbusch, *J. Phys. A* **38**, 5869 (2005).
- 21) H. Arisue, *Phys. Rev. E* **79**, 011107 (2009).
- 22) Y. Komura and Y. Okabe, *J. Phys. Soc. Jpn.* **81**, 113001 (2012).
- 23) R. Kenna, *Condens. Matter Phys.* **9**, 283 (2006).
- 24) M. Levin and C. P. Nave, *Phys. Rev. Lett.* **99**, 120601 (2007).
- 25) Z. Y. Xie, J. Chen, M. P. Qin, J. W. Zhu, L. P. Yang, and T. Xiang, *Phys. Rev. B* **86**, 045139 (2012).
- 26) A. Denblyker, Y. Liu, Y. Meurice, M. Qin, T. Xiang, Z. Xie, J. Yu, and H. Zou, *Phys. Rev. D* **89**, 016008 (2014).
- 27) S. Hong and D.-H. Kim, *Phys. Rev. E* **101**, 012124 (2020).
- 28) A. García-Saez and T.-C. Wei, *Phys. Rev. B* **92**, 125132 (2015).
- 29) K. Okunishi, T. Nishino, and H. Ueda, *J. Phys. Soc. Jpn.* **91**, 062001 (2022).
- 30) J. F. Yu, Z. Y. Xie, Y. Meurice, Y. Liu, A. Denblyker, H. Zou, M. P. Qin, J. Chen, and T. Xiang, *Phys. Rev. E* **89**, 013308 (2014).
- 31) C. Chatelain, *J. Stat. Mech.* **2014**, P11022 (2014).
- 32) J. Chen, H.-J. Liao, H.-D. Xie, X.-J. Han, R.-Z. Huang, S. Cheng, Z.-C. Wei, Z.-Y. Xie, and T. Xiang, *Chin. Phys. Lett.* **34**, 050503 (2017).
- 33) Y. Chen, Z.-Y. Xie, and J.-F. Yu, *Chin. Phys. B* **27**, 080503 (2018).
- 34) Z.-Q. Li, L.-P. Yang, Z. Y. Xie, H.-H. Tu, H.-J. Liao, and T. Xiang, *Phys. Rev. E* **101**, 060105 (2020).
- 35) C.-Y. Huang, Y.-C. Lu, and P. Chen, *Phys. Rev. B* **102**, 165108 (2020).
- 36) H. Ueda, K. Okunishi, K. Harada, R. Krčmár, A. Gendiar, S. Yunoki, and T. Nishino, *Phys. Rev. E* **101**, 062111 (2020).
- 37) A. Ueda and M. Oshikawa, *Phys. Rev. B* **104**, 165132 (2021).
- 38) S. Yang, Z.-C. Gu, and X.-G. Wen, *Phys. Rev. Lett.* **118**, 110504 (2017).
- 39) S. Iino, S. Morita, and N. Kawashima, *Phys. Rev. B* **100**, 035449 (2019).
- 40) Z.-C. Gu and X.-G. Wen, *Phys. Rev. B* **80**, 155131 (2009).
- 41) I. Bena, M. Droz, and A. Lipowski, *Int. J. Mod. Phys. B* **19**, 4269 (2005).
- 42) W. Janke and R. Kenna, *J. Stat. Phys.* **102**, 1211 (2001).
- 43) C. N. Yang and T. D. Lee, *Phys. Rev.* **87**, 404 (1952).
- 44) T. D. Lee and C. N. Yang, *Phys. Rev.* **87**, 410 (1952).
- 45) M. E. Fisher, in *Lecture Notes in Theoretical Physics*, ed. W. E. Brittin (University of Colorado Press, Boulder, 1965) Vol. 7C, Chap. 1, p. 1.
- 46) W. Janke and R. Kenna, *Comput. Phys. Commun.* **147**, 443 (2002).
- 47) C.-O. Hwang, *Phys. Rev. E* **80**, 042103 (2009).
- 48) J. C. S. Rocha, L. A. S. Mól, and B. V. Costa, *Comput. Phys. Commun.* **209**, 88 (2016).
- 49) B. V. Costa, L. A. S. Mól, and J. C. S. Rocha, *Comput. Phys. Commun.* **216**, 77 (2017).
- 50) D.-H. Kim, *Phys. Rev. E* **96**, 052130 (2017).
- 51) F. Dunlop and C. M. Newman, *Commun. Math. Phys.* **44**, 223 (1975).
- 52) Y. Liu, Y. Meurice, M. P. Qin, J. Unmuth-Yockey, T. Xiang, Z. Y. Xie, J. F. Yu, and H. Zou, *Phys. Rev. D* **88**, 056005 (2013).
- 53) K. Yoshiyama and K. Hukushima, *J. Phys. Soc. Jpn.* **89**, 104003 (2020).
- 54) S. Morita and N. Kawashima, *Phys. Rev. B* **103**, 045131 (2021).
- 55) G. Evenbly and G. Vidal, *Phys. Rev. Lett.* **115**, 180405 (2015).
- 56) G. Evenbly, *Phys. Rev. B* **95**, 045117 (2017).
- 57) M. Bal, M. Mariën, J. Haegeman, and F. Verstraete, *Phys. Rev. Lett.* **118**, 250602 (2017).
- 58) M. Hauru, C. Delcamp, and S. Mizera, *Phys. Rev. B* **97**, 045111 (2018).
- 59) H. Weber and P. Minnhagen, *Phys. Rev. B* **37**, 5986 (1988).
- 60) M. Fishman, S. R. White, and E. M. Stoudenmire, arXiv:2007.14822.